Construction and Building Materials 125 (2016) 892–904

Contents lists available at ScienceDirect

Construction and Building Materials

journal homepage: www.elsevier.com/locate/conbuildmat

Evaluation of freeze-thaw damage on concrete material and prestressed concrete specimens

Xiao-chuan Qin [a], Shao-ping Meng [a], Da-fu Cao [b], Yong-ming Tu [a,c,*], Natalia Sabourova [c], Niklas Grip [c], Ulf Ohlsson [c], Thomas Blanksvärd [c], Gabriel Sas [c], Lennart Elfgren [c]

[a] School of Civil Engineering, Southeast University, No. 2 SiPaiLou, XuanWu District, Nanjing 210096, China
[b] School of Civil Science and Engineering, Yangzhou University, No. 198 HuaYangXiLu, HanJiang District, Yangzhou 225127, China
[c] Division of Structural Engineering, Luleå University of Technology, SE-971 87 Luleå, Sweden

HIGHLIGHTS

- We study the microscopic and macroscopic freeze-thaw damage on concrete material.
- We investigate the freeze-thaw prestress loss of the bonded and unbonded specimens.
- Severe microscopic damages occur after 200 freeze-thaw cycles.
- Prestress loss from the intact to the completed damaged status is about 5% of σ_{con}.
- Influence of grouting on freeze-thaw prestress loss depends on grout damage status.

ARTICLE INFO

Article history:
Received 15 October 2015
Received in revised form 20 July 2016
Accepted 25 August 2016
Available online 1 September 2016

Keywords:
Concrete structures
Durability
Assessment
Deterioration
Damage

ABSTRACT

The pore structure of the hardened concrete and the microscopic changes of a few selected pores throughout the freeze-thaw test were investigated by a method combining RapidAir and digital metalloscope. Traditional tests were also performed to evaluate the macroscopic change caused by freeze-thaw cycles (FTCs). The investigation shows that the concrete material, of which the spacing factor is 0.405 mm and the air content is 2.38%, can still withstand more than 300 FTCs. Severe microscopic damages occurred after approximately 200 FTCs and the freeze-thaw damage were gradually aggravated afterwards. Prestress forces have a remarkable impact on the failure pattern under FTCs. It was further found that the compressive strength as an indicator is more reliable than the relative dynamic modulus of elasticity in evaluating the freeze-thaw damage on concrete material. In addition, the test and analysis show that the measured prestress losses of bonded specimen are larger than that of unbounded specimen under the attack of FTCs due to the duct grouting effect. The ultimate freeze-thaw prestress loss is about 5% of σ_{con} for both the bonded and unbonded specimens because the grouting cement paste will eventually be completely destroyed.

1. Introduction

Freeze-thaw cycles (FTCs) can cause severe deterioration in reinforced concrete structures and prestressed concrete structures due to the nature of porous structure in concrete material. The microscopic porous structure inside the concrete material makes it capable of absorbing and holding water [1]. As the ambient temperature drops below 0 °C, ice will form inside the pores of concrete and the volume of water and ice mixture will increase, introducing pore pressure inside the porous concrete material. If the tensile stress in concrete caused by pore pressure exceeds the tensile strength of the pore structure, freeze-thaw induced micro-cracks will occur. Then, as the ambient temperature rises above 0 °C, more water will be absorbed into the pores and new micro-cracks. Therefore, freeze-thaw damage will be aggravated during the next freezing process [2–5].

In order to find out the freeze-thaw damage mechanism of concrete material and to quantify this damage, experiments with the

* Corresponding author at: School of Civil Engineering, Southeast University, No. 2 SiPaiLou, XuanWu District, Nanjing 210096, China.
E-mail addresses: qinxc@seu.edu.cn (X.-c. Qin), msp1960@vip.sina.com (S.-p. Meng), dfcao@yzu.edu.cn (D.-f. Cao), tuyongming@seu.edu.cn (Y.-m. Tu), natalia.sabourova@ltu.se (N. Sabourova), niklas.grip@ltu.se (N. Grip), ulf.ohlsson@ltu.se (U. Ohlsson), thomas.blanksvard@ltu.se (T. Blanksvärd), gabriel.sas@ltu.se (G. Sas), lennart.elfgren@ltu.se (L. Elfgren).

http://dx.doi.org/10.1016/j.conbuildmat.2016.08.098
0950-0618/

help of advanced measuring techniques have been performed in recent years. The Scanning Electron Microscopy (SEM) is widely used in the investigation of concrete exposed to rapid freeze-thaw in water, which shed lights on the micro-cracking, water-transporting and self-healing mechanism of concrete material [6–9]. Similar to SEM, another feasible method to investigate the concrete material property is to inspect the concrete samples treated by Fluorescent Liquid Replacement (FLR) under an optical microscope, which produced more contrasting pictures of pores and micro-cracks [10–12]. Although the microscopic changes of concrete due to FTCs could be observed and evaluated with these methods, these microscopic changes cannot be monitored continuously in real time. The used samples will be discarded after each test while the new samples for microscopic observation must be sawed from the concrete specimens and then be polished to meet the microscopy requirements.

In addition to these direct observation methods, mercury intrusion porosimetry (MIP), low temperature calorimetry (CAL), X-ray computed tomography (CT), etc. were also employed to evaluate the pore systems [5,13–16]. The MIP is a quite simple test method. The operational principle is to describe the pore distribution according to the correlation between mercury pressure and pore volume. Before the MIP test, the concrete samples need to be dried, which would bring additional damages to the pore structure of samples. Compared with the MIP, the CAL is a better and very useful tool in investigating the pore structure in hardened concrete because the pre-drying process is not necessary. However, it should be noted that both the MIP and the CAL will introduce extra damages into pore structure: in the MIP test, the drying process and the high pressure applied to the sample can alter the pore structure; in the CAL test, ice formation in pores under the very low temperature (−60 °C) can also bring extra stress inside the sample [5,13]. Hence, these destructive methods might be inappropriate for the measurements of pore structure system in concrete. The CT technology is a promising non-destructive tool to obtain the 3D portrait of pores and cracks in concrete through image-reconstruction [12]. Sicat et al. [14] applied this technique in their tests and succeeded in obtaining the increase of the void ratio during FTCs. Although some CT images were shown in their research work, the nature of freeze-thaw damage in concrete, i.e. the initiation and propagation of micro-cracks, was not discussed. Besides, it is really a challenging task for the existing CT system to detect micro-cracks with width ranging from 10 to 50 μm in full-scale concrete specimens, and the concrete specimens are usually over 5 cm in laboratory dimension [12]. Considering the pros and cons of the above mentioned methods, a new method combining RapidAir and digital metalloscope was employed in this study to monitor the microscopic changes of a few selected pores throughout the completed freeze-thaw test.

The changes in microscopic structure of concrete material have significant influence on the macroscopic performances of the concrete specimen. In recent years, several research groups focused on the degradation of mechanical performances of concrete material, e.g. compressive strength, Young's modulus, etc., under the attack of FTCs. Shang et al. investigated the strength and deformation of plain concrete under uniaxial, biaxial, and triaxial compression after FTCs based on a series of experiments [17–20]. Duan, Jin, & Qian [21] proposed the stress-strain relationships of frozen-thawed confined and unconfined concrete specimens. Hasan, et al. investigated influence of freeze-thaw damage on the mechanical behaviour of concrete, such as the strength, stiffness, deformation capacity and the stress-strain relationship of frost-damaged concrete subjected to fatigue loading [1,22]. As a supplement to the freeze-thaw damage database and in order to investigate the correlation between the microscopic and macroscopic freeze-thaw damages, traditional tests, such as concrete compression test, surface check and relative dynamic modulus of elasticity (RDME) test, were also performed in this study.

With the development of experimental techniques, freeze-thaw tests were also performed on reinforced concrete members to investigate this deterioration effect on concrete structures on the basis of FTCs tests of concrete material. Diao, Sun, Cheng, & Ye [23] investigated the coupling effects of corrosive solution, FTCs, and persistent bending loads on the structural behaviour of reinforced concrete beams and reinforced air-entrained concrete beams respectively, and found that a persistent load together with FTCs would damage the beams more severely than pure FTCs. Zandi Hanjari, Kettil & Lundgren [24] tried to simulate the bending tests of frost-damaged reinforced concrete beams performed by Hassanzadeh & Fagerlund [25] with Diana finite element model analysis, in which the changes of failure mode and of failure load caused by internal freeze-thaw damage in the tests were well predicted. Although the above mentioned research have improved the understanding of freeze-thaw damaged concrete structures, further investigations are still necessary and some new tests have been carried out, for example, the test on the effect of FTCs on prestressed concrete structures. In the previous study of the authors' research group [26], the deterioration in flexural behaviours of prestressed concrete beams subjected to FTCs was reported. Moreover, the prestress losses of prestressed concrete beams due to FTCs were also measured and analysed by this group [2]. However, some important features of prestressed concrete structures under FTCs attack are still not clear. Little research has been carried out on the duct grouting effect on the prestress loss due to FTCs. Furthermore, even less research has been carried out on the remaining effective prestress in the concrete specimens after the concrete material is completely damaged by the FTCs attack. The study in this paper focuses on these key problems of prestressed concrete specimens under the attack of FTCs by using novel experimental methods.

In this work, an experimental programme comprised over 350 FTCs was performed on a series of small-scale and large-scale concrete specimens: (i) to continuously evaluate the microscopic and macroscopic freeze-thaw damages of concrete; (ii) to compare the prestress loss of bonded prestressed concrete specimen with that of unbounded when both of them are subjected to FTCs; and (iii) to analyse the prestress losses of post-tensioned concrete members subjected to FTCs from intact condition to concrete material failure condition. Moreover, it should be noted that in this paper the small-scale concrete specimen is used for the microscopic observations after freeze-thaw attack while the large-scale specimens are used for macroscopic tests.

2. Experimental programme

2.1. Materials

The components and mix design for the concrete material are specified in Tables 1 and 2. The measured cubic compressive

Table 1
Materials for the concrete mix.

Components	Materials
Cement	P·II, 42.5R
Water	Tap water
Fine aggregates	River sand, Fineness module 2.4
Coarse aggregates	Crushed stone, 5–20 mm
Fly ash	Class I fly ash
Additives	JM-9 composite water reducing agent

Note: 'P·II' represents 'Type II Portland cement'; 'JM-9' is the name of composite water reducing agent used for the concrete in this test (Jiangsu Sobute New Materials Limited, Nanjing, China).

Table 2
Concrete mix design and basic properties.

Ingredients and basic properties	Concrete
Cement (kg/m^3)	463
Water-cement ratio	0.38
River sand (kg/m^3)	599
Crushed stone (kg/m^3)	1139
Fly ash (kg/m^3)	62
Composite water reducing agent (kg/m^3)	8.93
Air content of fresh concrete (%)	2.5
28-day compressive strength (MPa)	66.55

Table 3
Physical and mechanical properties of the reinforcements.

Physical and mechanical Properties	Prestressing reinforcement	Longitudinal reinforcement	Transverse reinforcement
Diameter (mm)	5	5	3
Yield strength (MPa)	1500	762	897
Ultimate strength (MPa)	1710	976	1148
Young's modulus (GPa)	202	200	203

strength for the concrete at the age of 28 days was 66.55 MPa. Prestressing reinforcement was a 5 mm diameter low-relaxation steel wire with a nominal ultimate strength of 1570 MPa. Hot-rolled plain steel bar (HPB) of 5 mm and 3 mm diameter were used as the longitudinal reinforcement and the transverse reinforcement respectively. The physical and mechanical parameters of the reinforcements are shown in Table 3.

2.2. Specimens

In this study, two kinds of specimens were prepared, i.e. the small-scale specimen ($30 \times 30 \times 10$ mm^3) and the large-scale ones ($600 \times 100 \times 100$ mm^3). In order to observe the microscopic changes inside the concrete materials, one $30 \times 30 \times 10$ mm^3 concrete specimen, i.e. small-scale specimen, was cut from 28-day cube, as shown in Fig. 1(a). Furthermore, one $400 \times 100 \times 100$ mm^3 prismatic reinforced concrete specimen with a $200 \times 40 \times 40$ mm^3 rectangular cuboid hole as a special container was prepared to hold the small-scale specimens. This special concrete container can protect the small-scale specimens from over-variation in temperature during freeze-thaw test, as shown in Fig. 2. Moreover, there were four $600 \times 100 \times 100$ mm^3 post-tensioned concrete beams, i.e. large-scale specimens, as shown in Fig. 3. Among these four specimens: (i) two were post-tensioned by unbonded concentric prestress wires; and (ii) the other two by bonded concentric prestress wires. These four post-tensioned concrete specimens were named as A-u-F, A-u-U, A-b-F and A-b-U, respectively, where 'A' represents the 'axial prestressed specimen', 'u' represents the 'unbonded prestress wires', 'b' represents the 'bonded prestress wires', 'F' represents 'in the freeze-thaw chamber', and 'U' represents 'under the indoor environment'. The specimens placed in the freeze-thaw chamber, i.e. the test group specimens A-u-F and A-b-F, were used to test the total prestress loss ($\Delta\sigma_l$), while the others, i.e. the control group specimens A-u-U and A-b-U, were exposed to the indoor environment to measure the prestress loss caused by other factors ($\Delta\sigma_{lO}$) such as shrinkage and creep, etc. The prestress loss of the test group specimens minus that of the control group specimens was used to estimate the prestress loss due to the FTCs ($\Delta\sigma_{lF}$). Besides, three

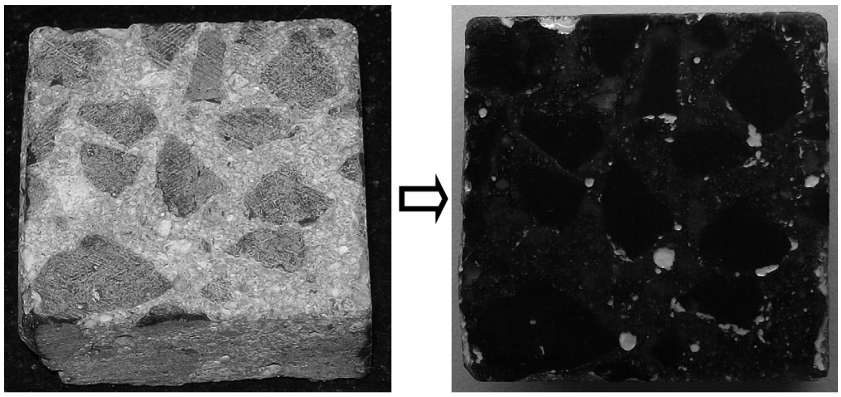

Fig. 1. Small-scale specimen for microscopic observation.

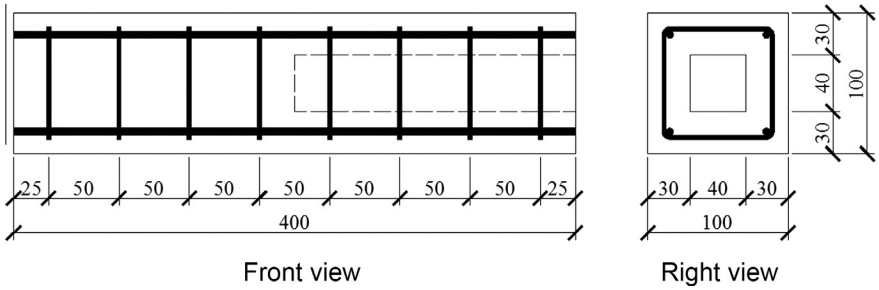

Fig. 2. Concrete container.

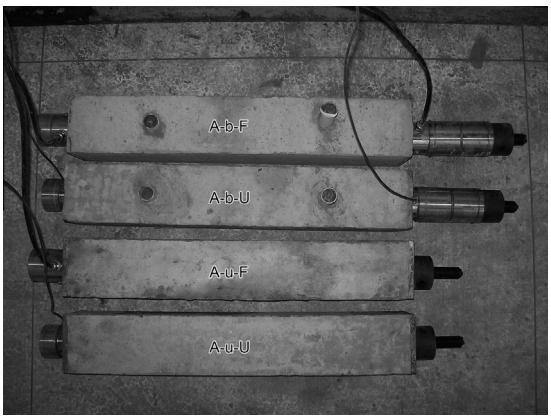

Fig. 3. Axial prestressed concrete specimens.

$400 \times 100 \times 100\ mm^3$ prisms and sixteen groups of 100 mm cubes (three cubes as a group, totally forty-eight cubes) made of plain concrete were prepared to investigate the deterioration of concrete material properties under the attacks of designated number (0, 25, 50, . . ., 350) of FTCs. It should be noted that the first group of cubes were tested after 28 days' cure to obtain a standard compressive strength and to make sure the concrete was strong enough to be prestressed, and the other fifteen groups were tested after the 0th, 25th,50th,. . .,350th freeze-thaw cycle (FTC) respectively.

2.3. Programme

2.3.1. Mixing, air content and curing of concrete material

All specimens were cast by the same concrete material and then cured under the standard curing condition. The preparation steps for concrete material include: (1) all the ingredients of concrete except water were mixed for 30 s; (2) then water together with the mixture of the above-mentioned ingredients was mixed for 3 min; (3) the freshly mixed concrete was poured into steel moulds and then vibrated for 30 s on the vibrating table; (4) at the same time, the air content of fresh concrete was tested by LC-615A air meter (Sanyo Testing, Japan); and (5) the concrete specimens were cured under 20 °C and RH 95% for 28 days and then stored under the indoor environment.

2.3.2. RapidAir test of concrete material

The pore distribution test was carried out according to the User's Manual of RapidAir 457 [27]. Firstly, the small-scale specimen was cut from matured concrete with a concrete saw, as close to parallel planes as possible. Secondly, the small-scale specimen was ground with 240# silicon carbide abrasive paper so that the roughness of the specimen was removed and the surface is very plane. Thirdly, the specimen was polished by using 400#, then 800#, and then 2000# silicon carbide abrasive paper in sequence in a special solution of sulfo-soap and water. To avoid blocking the pores by dust the specimen must be cleaned with a soft brush under running water after each step. After the surface smoothness of the small-scale specimen was checked by the stereomicroscope and met the requirements of RapidAir test, the specimen was coloured black using a broad tip marker pen. Afterwards, the specimen was heated to about 55 °C to help the white zinc paste massaged onto the polished surface to melt and flow by itself into the voids. Then the specimen was placed in a refrigerator at 5 °C for approximately 10 min. Excess zinc paste was removed from the cooled surface by a straight edge knife. Again, the specimen surface was checked by the stereomicroscope to ensure the concrete void was fully filled with zinc paste, the edge of voids was clear and the contrast ratio of white voids to black paste was good enough. The prepared specimen (see Fig. 1(b)) was then fixed on the sample holder to perform the RapidAir test, as shown in Fig. 4(a).

2.3.3. Preparation of prestressed concrete specimens

The concrete specimens were prestressed by the hydraulic actuator, and the prestress steel wires were anchored by the button-head anchorage system. The nominal stress in the wires is about 65% of the ultimate strength of wires. In order to counterbalance the prestress relaxation losses, the prestress wires were over-stretched to 1.03 times of the nominal prestress. A CCG annular load cell (Applied Measurements Limited, Berkshire, UK) was installed at the anchoring end of each specimen to record the prestress forces. For A-b-F and A-b-U, an additional load cell was installed at the tensioning end, as shown in Fig. 3, to investigate whether and how the duct grouting quality influences the prestress loss due to FTCs. The bonded specimens, A-b-F and A-b-U, were injected with cement paste immediately after the steel wires had been prestressed. It was three weeks after the two bonded specimens had been grouted that the test group specimens A-b-F and A-u-F were placed into the freeze-thaw chamber to perform the Rapid Freeze-Thaw in Water Test, while the control group specimens, i.e. A-b-U and A-u-U, were placed under the indoor environment. The test group specimens were immersed in water for 48 h prior to FTCs. The control group specimens were coated with two layers of saturated cotton gauzes and then with six layers of plastic films to ensure these two specimens experienced approximately the same relative humidity as those stored inside the chamber. Furthermore, the relative humidity of the control group specimens were monitored in real time by the thermo-hygrometer attached to the specimen's surface, as shown in Fig. 5.

2.3.4. Freeze-thaw test

Together with the prestressed concrete specimens, the prismatic concrete container holding the small-scale specimen, the concrete prisms and the cubes were placed into the freeze-thaw

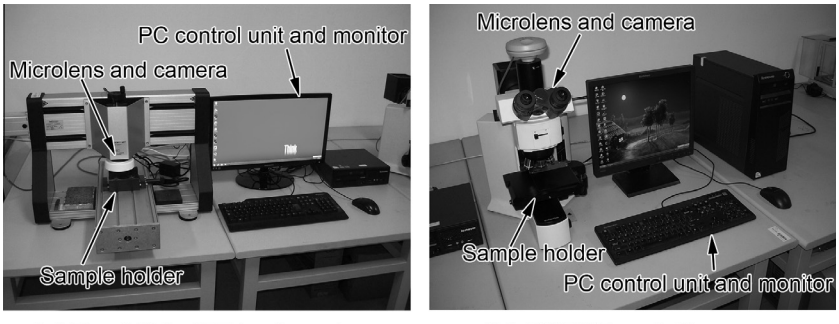

Fig. 4. RapidAir 457 test system and BX51M metalloscope.

Fig. 5. Freeze-thaw test apparatus and control group specimens A-b-U and A-u-U monitored in real time by the thermo-hygrometer.

chamber. The freeze-thaw test was carried out according to the ASTM C666-03 [28] Procedure A. The procedure of this FTCs test mainly includes the following two steps: (1) the temperature of the specimens was linearly decreased from +5 °C to −16 °C over a time duration of 2.0 h; and (2) then it was linearly increased from −16 °C to +5 °C over a period of 1.0 h. This means that two thirds of the time duration of one FTC was used for freezing while one third for thawing. Moreover, it took about 1.7 h to decrease the core temperature of a specimen from +3 °C to −16 °C while 0.95 h to increase it from −16 °C to +3 °C. The duration of transition between the freezing and thawing phases of one cycle was about 5 min. As described above, the annular load cells connected to an electric resistive indicator (Yangzhou Test Limited, Yangzhou, China) were used to measure the prestress forces applied by the prestressing steel wires, as shown in Fig. 5. The prestressing forces were recorded at the points in time when the centric temperature of the specimen reached 5 °C every 25 FTCs. At the same time, the small-scale specimen was taken out from the prismatic concrete container and then observed under the BX51M metalloscope (Olympus, Japan), as shown in Fig. 4(b). Meanwhile, three 100 mm concrete cubes were taken out from the freeze-thaw chamber to perform the concrete material compression test. Three concrete prisms were also taken out to perform a series of non-destructive tests, such as concrete surface inspection and test of RDME. Afterwards, the small-scale specimen and the three prisms were put back into the prismatic concrete container again to experience the following 25 FTCs.

3. Experiment results

3.1. Air content and pore distribution

The air content of hardened concrete, the specific surface, void frequency, spacing factor, and paste-air ratio of the air-void system in hardened concrete are listed in Table 4. The air content of hardened concrete given by the RapidAir test is 2.38%, slightly less than the air content of fresh concrete obtained by LC-615A air meter, see also Table 2. Among all the parameters measured by the RapidAir test, the spacing factor is the most significant indicator of freeze-thaw durability of concrete specimens. The value of spacing factor in this test, 0.405 mm, is larger than the maximum value for moderate freeze-thaw exposure, 0.20 mm. Furthermore, the frequency of chord length and the air content are shown in Fig. 6. Although the pores smaller than 0.10 mm frequently appeared under the microscope, they contributed very little to the total air content. However, the pores larger than 2.0 mm contain 0.53% air, more than 20% of the total air content.

Table 4
Test results of RapidAir.

Parameter	Value
Air Content (%)	2.38
Specific Surface (mm^{-1})	19.68
Spacing Factor (mm)	0.405
Void Frequency (mm^{-1})	0.117
Average Chord Length (mm)	0.203
Paste to Air Ratio	16.81

3.2. Micro- and macro-freeze-thaw damage

3.2.1. Damage on pore structure

The evolution of pore expansion and micro-cracking of the representative pores under FTCs attack are shown in Figs. 7–9.

The smallest pore radius monitored by the metalloscope was about 65 μm. It was surrounded by three pores, one about 400 μm and two about 100 μm in radius. These four pores were marked by numbers 1, 2, 3 and 4, as shown in Fig. 7. This region was damaged very fast during the first 50 FTCs and the areas of these four pores increased respectively after the 50th FTC. Moreover, the trends of cracking were also observed between the pores No. 1, No. 2 and No. 3, and the crack width was about 8 μm. As FTCs were repeated, the size of these pores continued to increase. After the 100th FTC, the pore No. 1 was connected with the pores No. 2, No. 3 and No. 4 because of the rapid growth of cracks and concrete scaling due to FTCs attack. The width of the surface cracks increased sharply after the 200th FTC, and pore No. 3 and pore No. 4 were connected with each other by a deep and wide crack. At the final stage of the FTCs test, i.e. after the 325th FTC, the cracks among the pores No. 2, No. 3 and No. 4 became even deeper, which indicated the concrete material was approaching ruptured.

One medium size pore together with part of an interface zone (ITZ) is shown in Fig. 8. The pore size only increased slightly from the 0th FTC to the 100th FTC, while the dimension of the ITZ hardly changed before the 175th FTC. However, one clear 50 μm wide crack was observed after the 200th FTC, and the width of this crack grew to about 130 μm after the 325th FTC. Along with this crack, another narrow crack, which started from the ITZ on the right side and ended at the sand gravel on the lower-left side of the figure, occurred after the 325th FTC. The area of this medium-size pore increased about 65% after the 325th FTC.

The freeze-thaw damage on a relatively large single pore is shown in Fig. 9. The pore radius in this figure was about 700 μm. Significant freeze-thaw damage other than pore size increase was observed during the last 125 FTCs. After the 200th FTC, a blurry narrow crack was observed near the bottom-right side of the pore under the metalloscope, which is about 2 μm wide. After that, this part of the pore edge was ruptured due to the growth of this crack at around the 275th FTC. During the following FTCs, the bottom-right part of the pore edge was gradually ruptured, which finally led to failure of the pore structure.

After the 350th FTC, the small-scale specimen was ruptured into pieces due to freeze-thaw penetrating cracks, as shown in Fig. 10(a).

3.2.2. Scaling and splitting of large-scale concrete specimens

The three concrete prisms have hardly scaled during freeze-thaw test, which was different from the small-scale specimen. All the prisms, No. 1, No. 2 and No. 3, bended very slightly after the 300th FTC, and only a few short flexural cracks and surface pores occurred on the bottom surface of the prisms. Moreover, these cracks and surface pores were so tiny that they are not easily observed, as show in Fig. 10(b), (c) and (d). Although the damage

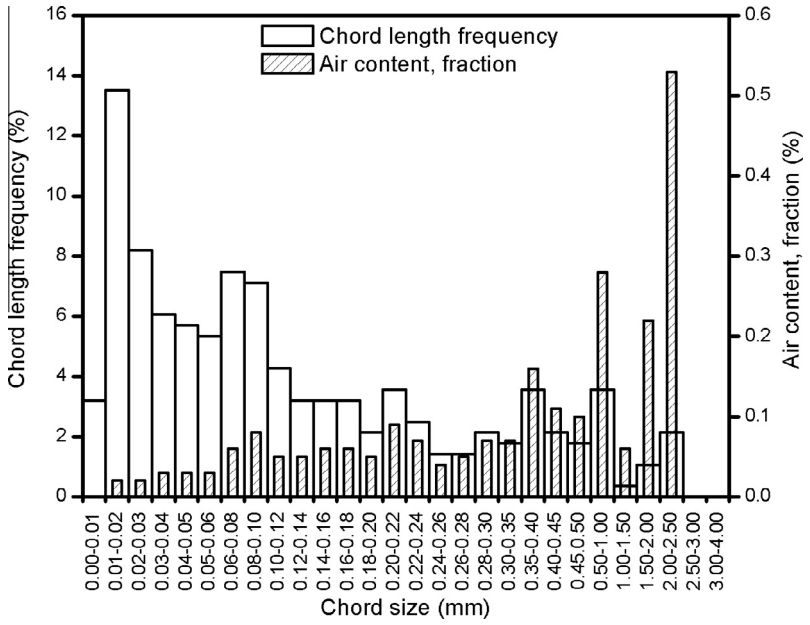

Fig. 6. Histograms of chord length frequency and the air content.

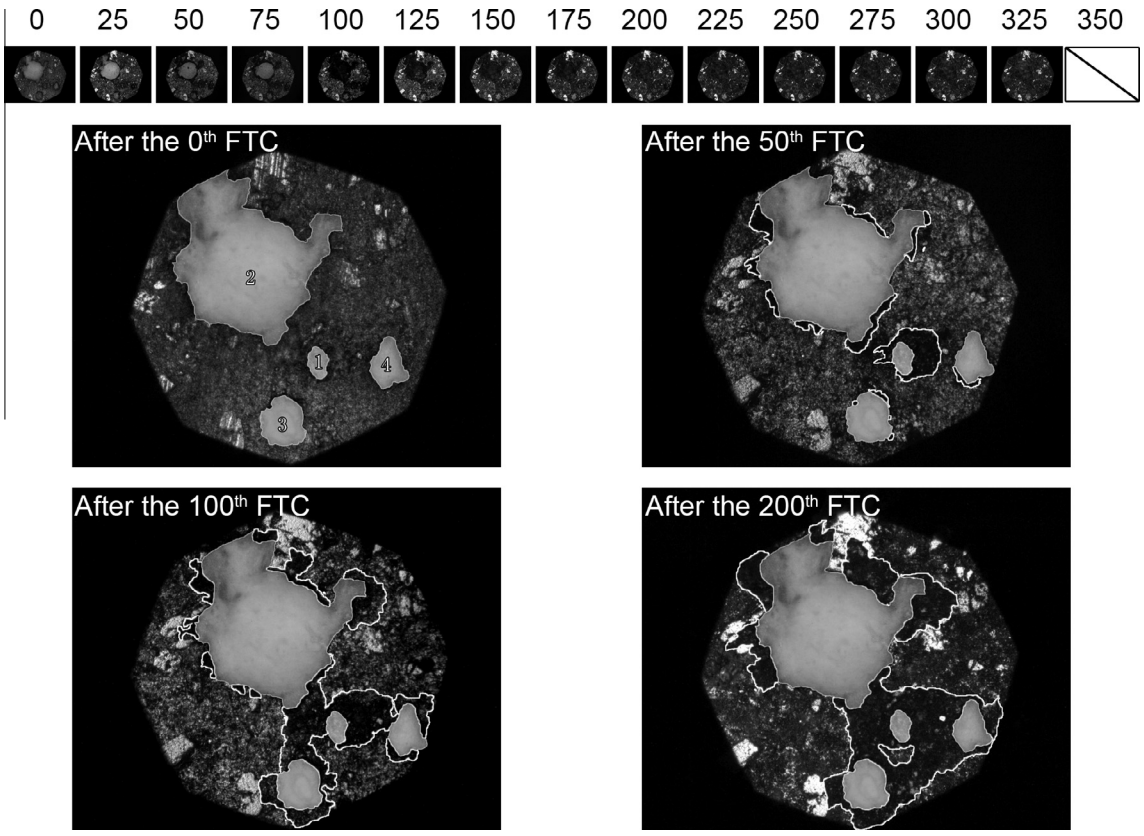

Fig. 7. Freeze-thaw damage on small pores. Note: The radius of pores 1–4 in up-left figure are about 65 μm, 400 μm, 100 μm and 100 μm respectively.

of the concrete prisms were little after 300 FTCs, the prisms underwent great changes after the 350th FTC, i.e. at the end of freeze-thaw test, and one concrete prism was split at the top middle surface, as shown in Fig. 10(e). Meanwhile, the 16th group of cubes for testing mechanical properties of concrete material were ruptured due to freeze-thaw cycle attack, as shown in Fig. 10(f), which also meant that no compressive strength information of the concrete material under more than 350 FTCs attack was obtained in this investigation. Another interesting phenomenon at the end of the freeze-thaw test was that the scaling of prestressed specimens was serious, as shown in Fig. 11. Both the bonded specimen (A-b-F) and the unbounded specimen (A-u-F) scaled approximately to the same extent, while no splitting or rupture of these two specimens occurred after the 350th FTC.

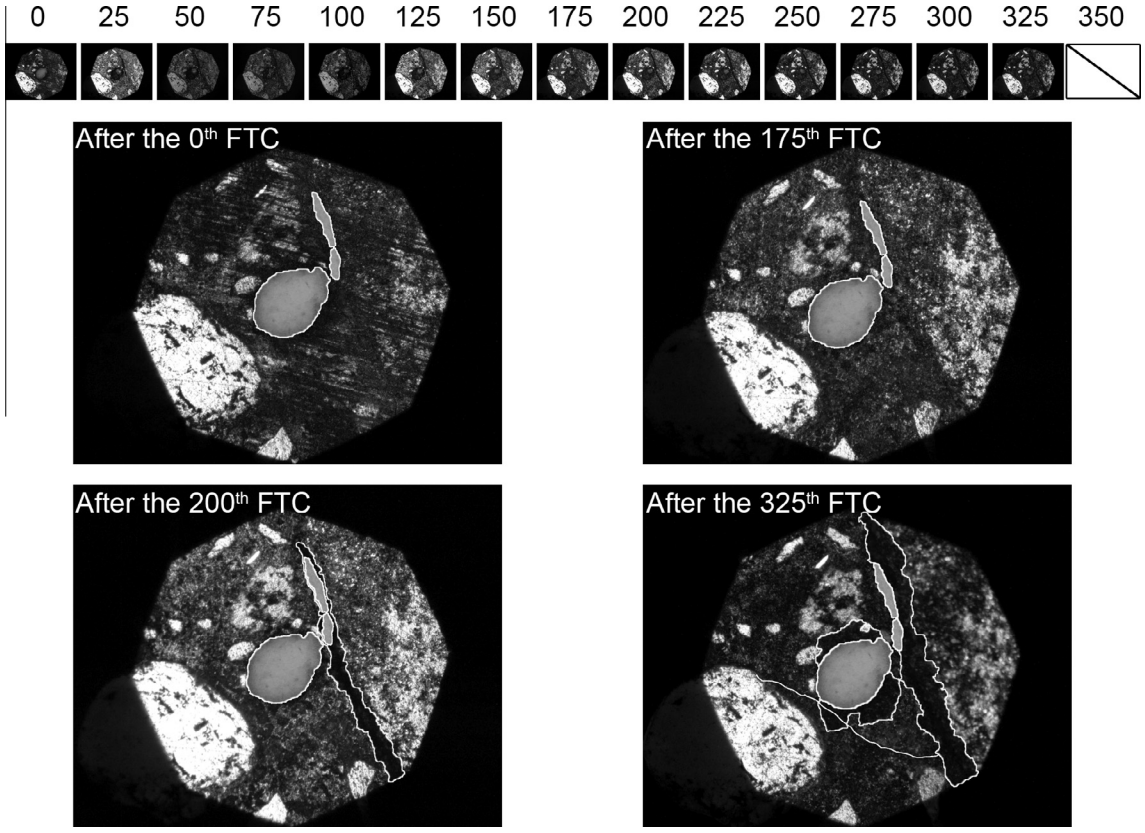

Fig. 8. Freeze-thaw damage on medium-size pore and ITZ. Note: The radius of the medium-size pore is about 200 μm.

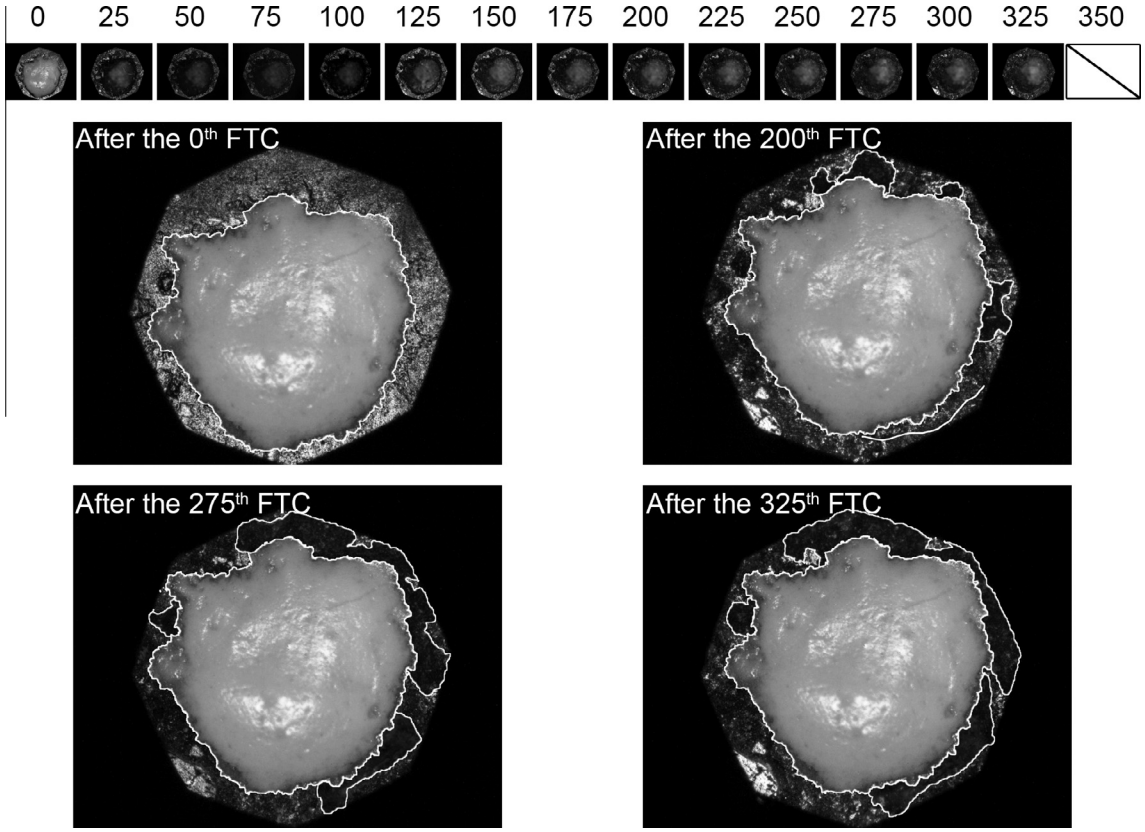

Fig. 9. Freeze-thaw damage on large single pore. Note: The radius of the large single pore is about 700 μm.

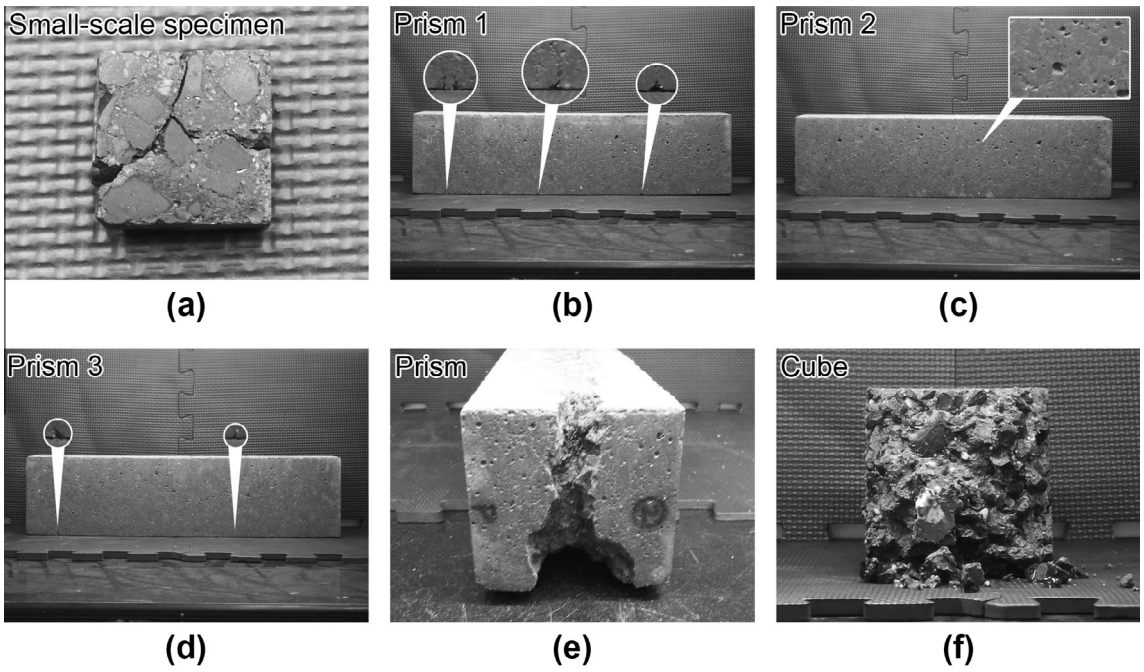

Fig. 10. Freeze-thaw damage on concrete material.

3.3. Strength, Young's modulus and RDME

The compressive strength, Young's modulus and RDME of concrete material damaged by FTCs are listed in Table 5. The deterioration trends of concrete under FTCs are shown in Fig. 12. The last three concrete cubes was broken into pieces while the prisms split at the top middle surface after the 350th FTC, so the results for this FTC could not be obtained. Besides, it can be seen that the compressive strength and Young's modulus decreased as FTCs were repeated and both decreased sharply after the 275th FTC. However, the RDME dropped sharply at around the 50th FTC, and then only around 15% of initial RDME value remained after the 175th FTC. After that the RDME fluctuated around 15% level for the following 125 FTCs and then decreased again.

3.4. Prestress losses

In this section, the prestress losses of the test specimens under the attack of FTCs are analysed, mainly including: (i) the prestress losses of the specimens due to FTCs $\Delta\sigma_{lF}$, (ii) the prestress losses of

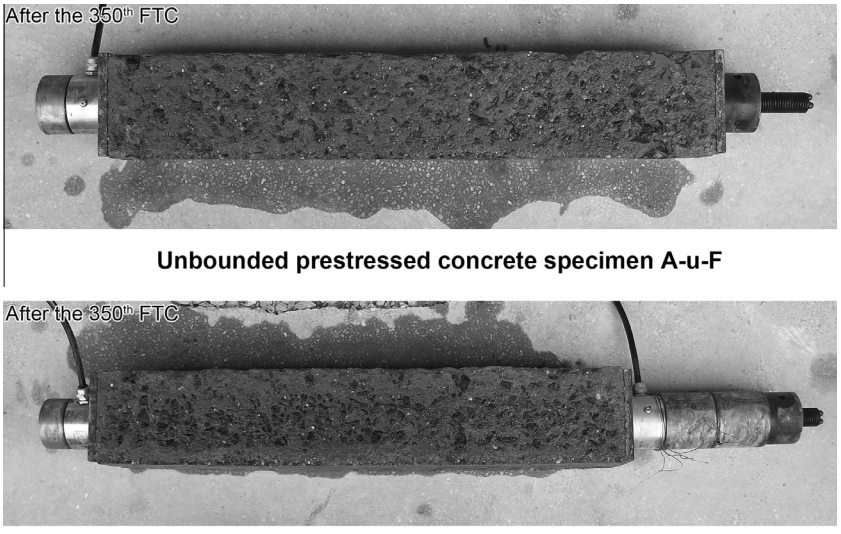

Fig. 11. Freeze-thaw damaged prestressed concrete specimen.

Table 5
Properties of concrete material damaged by FTCs.

FTCs	Compressive strength		Young's modulus		RDME
	Abs. (MPa)	Rel. (%)	Abs. (GPa)	Rel. (%)	(%)
0	70.6	100.00	36.3	100.00	100.00
25	69.6	98.62	36.2	99.67	98.52
50	67.6	95.69	35.9	99.01	96.79
75	65.6	92.93	35.7	98.31	86.65
100	64.4	91.15	35.5	97.85	71.74
125	62.2	88.13	35.2	96.98	52.50
150	60.8	86.08	35.0	96.36	39.28
175	58.2	82.42	34.6	95.39	19.11
200	55.3	78.31	34.2	94.21	15.73
225	53.2	75.36	33.9	93.25	16.64
250	50.8	72.00	33.4	92.00	14.15
275	48.3	68.36	32.9	90.55	15.75
300	43.5	61.65	31.8	87.48	12.92
325	30.8	43.69	27.4	75.44	5.80
350	–	–	–	–	–

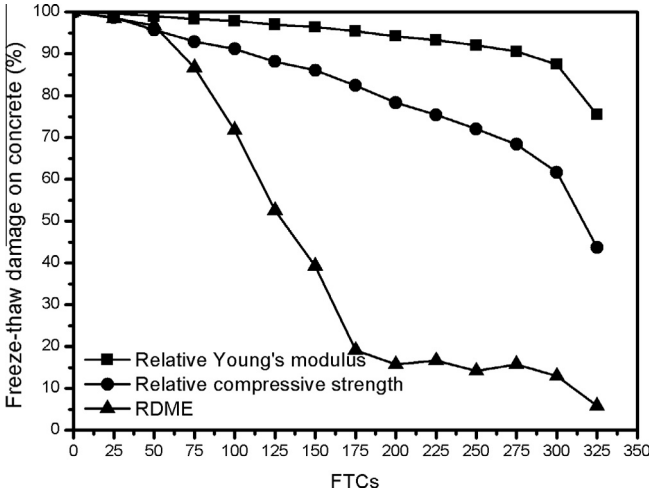

Fig. 12. Deterioration trends of Young's modulus, compressive strength and RDME of concrete under FTCs.

the test group specimens placed inside the freeze-thaw chamber, $\Delta\sigma_l$, which consist of the losses both from FTCs ($\Delta\sigma_{lF}$) and from the other factors, and (iii) the prestress losses of the control group specimens placed outside the freeze-thaw chamber, $\Delta\sigma_{lO}$, which was obviously equal to $\Delta\sigma_l - \Delta\sigma_{lF}$. It should be noted that in the following notations, the superscript *A-u* and *A-b* represent the unbounded and the bonded specimens respectively; and the superscript τ and α represent the tensioning end and the anchoring end respectively. For example, $\Delta\sigma_{lO}^{A\text{-}b,\ \alpha}$ means the prestress losses of A-b-U at the anchoring end.

The measured prestress losses of the four prestressed specimens are summarized in Table 6, including the prestress losses of the test group specimens A-u-F and A-b-F ($\Delta\sigma_l$) and that of the control group specimens placed under the indoor environment, A-u-U and A-b-U ($\Delta\sigma_{lO}$). The results of A-u-F ($\Delta\sigma_l^{A\text{-}u}$) are a bit smaller than that of A-b-F ($\Delta\sigma_l^{A\text{-}b,\ \tau}$ and $\Delta\sigma_l^{A\text{-}b,\ \alpha}$). Furthermore, the results of A-b-F at the anchoring end of anchorage system ($\Delta\sigma_l^{A\text{-}b,\alpha}$) is very close to that at the tensioning end ($\Delta\sigma_l^{A\text{-}b,\ \tau}$) and the largest difference between them is only 1.26 MPa. After the specimen A-b-F experienced more than 250 FTCs, the difference between the prestress losses at the tensioning end and that at the anchoring end gradually disappeared.

The measured prestress losses due to FTCs in this test (i.e. $\Delta\sigma_{lF}^{A\text{-}u}$, $\Delta\sigma_{lF}^{A\text{-}b,\ \tau}$ and $\Delta\sigma_{lF}^{A\text{-}b,\ \alpha}$) are shown in Fig. 13. The predictions according to a previous work [2] are also included in Fig. 13. For a better view of the difference between the measurements and predictions, the measured and predicted results of $\Delta\sigma_{lF}^{A\text{-}u}$, $\Delta\sigma_{lF}^{A\text{-}b,\ \tau}$ and $\Delta\sigma_{lF}^{A\text{-}b,\ \alpha}$ are plotted in three separate smaller graphs respectively, as shown

Table 6
Prestress losses of prestressed concrete specimens.

FTCs	Unbounded specimens		Bonded specimens			
	$\Delta\sigma_{lO}^{A\text{-}u}$ (MPa)	$\Delta\sigma_l^{A\text{-}u}$ (MPa)	$\Delta\sigma_{lO}^{A\text{-}b,\ \tau}$ (MPa)	$\Delta\sigma_{lO}^{A\text{-}b,\ \alpha}$ (MPa)	$\Delta\sigma_l^{A\text{-}b,\ \tau}$ (MPa)	$\Delta\sigma_l^{A\text{-}b,\ \alpha}$ (MPa)
0	0.00	0.00	0.00	0.00	0.00	0.00
25	0.00	0.00	0.00	0.00	0.70	0.68
50	0.76	1.41	0.86	0.00	1.39	2.04
75	1.51	2.12	0.86	2.25	2.79	3.39
100	1.51	2.12	1.72	2.25	3.49	4.75
125	2.27	3.53	1.72	3.01	4.88	5.43
150	3.02	4.23	1.72	3.76	5.58	6.11
175	3.78	4.94	3.43	3.76	6.28	6.78
200	4.53	6.35	3.43	4.51	6.97	7.46
225	5.29	7.05	4.29	5.26	7.67	8.14
250	5.29	7.76	4.29	6.01	8.37	8.82
275	5.29	8.46	5.15	6.01	9.07	8.82
300	5.29	9.87	5.15	6.76	11.16	10.85
325	5.29	14.10	5.15	6.76	15.34	14.93
350	5.29	55.71	5.15	6.76	56.49	56.31

Note: $\Delta\sigma_{lO}^{A\text{-}u}$ represents the prestress losses of A-u-U; $\Delta\sigma_l^{A\text{-}u}$ represents the prestress losses of A-u-F; $\Delta\sigma_{lO}^{A\text{-}b,\ \tau}$ represents the prestress losses of A-b-U at the tensioning end; $\Delta\sigma_{lO}^{A\text{-}b,\ \alpha}$ represents the prestress losses of A-b-U at the anchoring end; $\Delta\sigma_l^{A\text{-}b,\ \tau}$ represents the prestress losses of A-b-F at the tensioning end; and $\Delta\sigma_l^{A\text{-}b,\ \alpha}$ represents the prestress losses of A-b-F at the anchoring end.

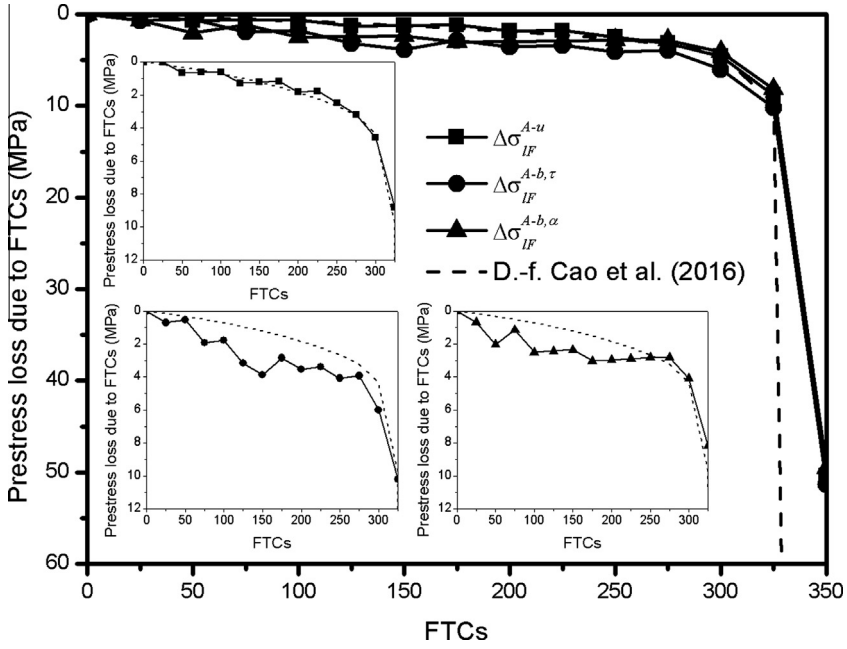

Fig. 13. Prestress losses of concrete specimen due to FTCs.

in Fig. 13. For the unbonded specimen A-u, the predictions agree with the measured freeze-thaw prestress losses ($\Delta\sigma_{lF}^{A-u}$) quite well for the first 325 FTCs. When approaching the 350th FTC the deviations between the predictions and test results become obvious. Moreover, both the predicted and measured results drop sharply from the 325th to the 350th FTC. Since the concrete cubes and the prisms are ruptured after 350 FTCs attack, the corresponding mechanical properties of concrete material under this condition are not available, which result in the unpredictable deviations when applying the equations [2] to predict the prestress loss. For the bonded specimen, the measured prestress losses ($\Delta\sigma_{lF}^{A-b,\ \tau}$ and $\Delta\sigma_{lF}^{A-b,\ \alpha}$) at both the tensioning end and the anchoring end gradually decrease and fluctuate from the 50th FTC to the 250th FTC. Then the measured results drop sharply from the 275th to 325th FTC, which is very similar to the case of unbonded specimens. The relatively large deviation between measured results and predictions is also observed after the 350th FTC due to lack of the knowledge of the mechanical properties of concrete material.

4. Discussions

4.1. Impact of external stress on the failure of concrete specimens

Figs. 10(e), (f) and 11 show quite different failure patterns of concrete material: the plain concrete specimens, including prisms and cubes, hardly scaled before the 350th FTC attack, but after that FTC they were split or ruptured. However, although the prestressed specimens scaled severely after the 350th FTC, they were never ruptured or split. This difference might be attributed to the different stress state of concrete material. During the hardening process of the concrete, internal cracks formation mainly occur in the cement paste and the paste-aggregate interface transition zone (ITZ) due to various factors, such as shrinkage of cement paste, temperature, etc. When the concrete specimen is immersed in water, it will absorb water into the concrete's pore system. As the temperature drops below the freezing point of water, the water will turn into ice accompanied by a 9% volume increase, which causes tensile stress inside the concrete.

If no external stress is applied to the concrete specimen, new micro-cracks will form in local region where the tensile stress is higher than the tensile strength of concrete material. Then, more water will be absorbed into this concrete region with micro-cracks during thawing, which causes larger expansion and more internal cracks in concrete during the next FTC. Such freeze-thaw damage will be aggravated in the local region as the FTCs are repeated.

On the other hand, if an external force is applied to the concrete specimen, the distribution of stress in concrete will alter. This means that the external force can introduce compressive stress into local part of concrete specimen which will counterbalance part of the tensile stress by the action of ice formation and expansion. On the contrary, the external force can also introduce tensile stress into other local part of specimen which will be superimposed on the tensile stress from ice. Hence, the crack occurrence and propagation of concrete specimens will be influenced by such stress counterbalance or superimposition. This is why plain concrete specimens and prestressed specimens show the different freeze-thaw failure patterns although they were made of the same concrete. For concrete structural members, such as beams and columns, the stress state as well as the freeze-thaw effect will influence the cracking and failure pattern. Tensile stress in the tension zone of beams will result in more localized surface scaling, wider and longer flexural cracks which have been reported by Diao et al. [23]. Axial compressive stress in columns will make the cover zone under radial tensile stress state, which will lead to more scaling after FTCs, as shown in Fig. 11.

4.2. Evaluation of freeze-thaw damage

In the assessment of the freeze-thaw damage on concrete, various indicators of damage, such as RDME and compressive strength, should be measured in each individual case. The RDME can be evaluated by fundamental transverse frequency tests on concrete prisms. The compressive strength can be evaluated by compression tests on concrete cubes or drilled cores. In addition, it is believed that a correlation exists between the loss of RDME and the degradation of compressive strength [24,29,30]. However,

it is very difficult to find the appropriate regression curves for them. For example, when the compressive strength of concrete cube drops from 60 MPa to 40 MPa, the corresponding RDME might drop from 100% to 95%, or even to 30% [24]. The variation trend of the RDME differs from that of the compressive strength in this experiment, as shown in Fig. 12. This phenomenon also shows these two factors assess the freeze-thaw damage of concrete material in different aspects, respectively. It is clearly observed that from Figs. 7–9 and 12, microscopic freeze-thaw damages, such as cracks in pore structure and ITZ in concrete, usually occur after the 200th FTC. At this moment, the RDME dropped from 100% to about 15%, while the compressive strength remained more than 75% of its initial value. This difference is believed to be caused by the measuring mechanism of RDME.

The test of RDME is developed from the analysis of a homogeneous rod under free flexural vibration, which assumes that the specimen is homogeneous and elastic. However, this assumption is not quite true for concrete material, especially for freeze-thaw damaged concrete material. As shown in Fig. 14, although there are pores and micro-cracks in the undamaged concrete, the volume ratio of these inherent defects to the specimen is very small. When the concrete specimen is under this well condition, the vibration wave can transit through it easily. Hence, it is reasonable to consider the undamaged concrete specimen as homogeneous and elastic. Nevertheless, as FTCs go on, the original micro-cracks in the specimen will propagate and at the same time new cracks will occur. These deep and wide micro-cracks tend to separate the specimen into a few parts. Thus, the specimen cannot be treated as a homogeneous material any more, which conflicts with the basic assumption of RDME measuring mechanism. This is also the reason why the lower bound of RDME should be equal to or greater than 60% of its initial value according to the rules given in the test standards such as ASTM C666 [28], GB/T50082 [31], etc. If the RDME decreases to 60% of the initial value, the specimen is tagged "Failure". This "Failure" is actually the failure of microscopic pore structure, which is supported by Figs. 7 and 12. The microscopic damages observed in Fig. 7 were in good accordance with the loss of RDME shown in Fig. 12. Before the RDME started to drop sharply, i.e. before the 50th FTC, the initial microscopic damages occurred at the edge of each pore. However, it should be noted that these micro-cracks were not connected with each other at this time. From the 50th to the 175th FTC, the damaged regions were connected with each other by micro-cracks' propagation while the RDME dropped sharply from about 95% to 15%. However, as shown in Figs. 8 and 9, few damages were observed before the 200th FTC because these pores were relatively far from the others. This phenomenon indicates that the RDME is sensitive to the formation and propagation of micro-cracks in the region where pores are close to each other. Hence, the RDME is only an appropriate indicator for internal pore structure and it is suitable for the application of concretes which are slightly damaged by FTCs.

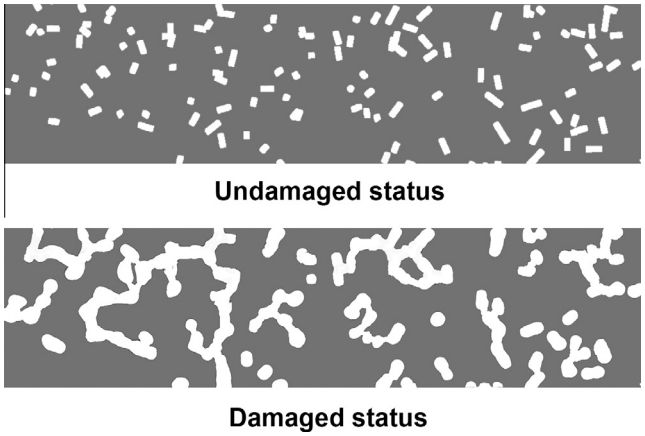

Fig. 14. Development of micro-defects of the concrete under FTCs damage.

On the other hand, the compressive strength seems more reliable for both the intact concrete and the severely damaged concrete. Taking the large single pore in Fig. 9 as an example, it was around from the 275th FTC to the 325th FTC that the pore structure was ruptured by the freeze-thaw induced cracks, and it was also approximately at the same time that the compressive strength of concrete specimen decreased sharply, as shown in Fig. 12. This implies that the compressive strength of concrete material is more suitable for evaluating the macroscopic freeze-thaw damage of concrete. In the compression test, the concrete material is usually assumed to be homogeneous while actually it is not homogeneous but composed of several different types of materials, such as aggregates and cementitious material. There are always internal micro-defects in the concrete, especially near the interfacial transition zones (ITZs) between the cementitious paste and aggregates. In an earlier concrete compression test [33], the freeze-thaw damaged concrete exhibited a considerably lower initial elastic modulus compared to the undamaged concrete, and the ascending branch of the stress-strain curve also showed the corresponding change in the stiffness. This is believed to be caused by freeze-thaw induced cracks. Some of the freeze-thaw induced cracks (i.e. the cracks approximately perpendicular to the compressive force) will firstly be compacted by the compressive force from the test machine before the concrete is ruptured, which can be regarded as a process of 'crack closure'. This illustrates that the FTCs induced cracks in concrete have less impact on the compressive strength of concrete.

Based on the above-mentioned measurements and analysis, the compressive strength of concrete is proved to be more suitable and reliable than the RDME to evaluate the concrete damage by FTCs. In addition, it should be noted that the RDME of concrete tends to recover if it is not measured immediately after the FTCs end, especially that of high-strength concrete. Due to low water-cement ratio, the high-strength concrete likely contains un-hydrated cement which will continue the hydration process. The hydration process will reduce the available amount of free water for freeze-thaw process and produce additional cementitious paste to repair the micro-cracks in the concrete specimen, so the RDME of high-strength concrete is apt to self-recover. Nevertheless, the hydration process has relatively less effect on the compressive strength of concrete material than on RDME as time is going on. In Jacobsen & Sellevold's research work [32], experimental results showed that the concrete specimens deteriorated by rapid freeze-thaw in water could almost fully recover the loss of resonance frequency under subsequent water storage condition. However, the compressive strength recovered only 4–5% during healing after an initial loss of 22–29% due to freeze-thaw damage. In a word, the compressive strength of concrete material is a more reliable indicator, which can reflect the response of the freeze-thaw damaged concrete structure more clearly and accurately.

4.3. Prestress losses due to FTCs

In the post-tensioned prestressed concrete specimens, almost no compressive prestress could exist in the duct grouting because the cement paste in flow condition was injected into the duct right after stretching the prestressing wires. When the cement paste was in the process of hardening, the prestress force was still carried by the concrete and little compressive stress was transferred to the cement paste. That is to say, the duct grouting contributed little to resisting the compressive force applied by the prestressing wires.

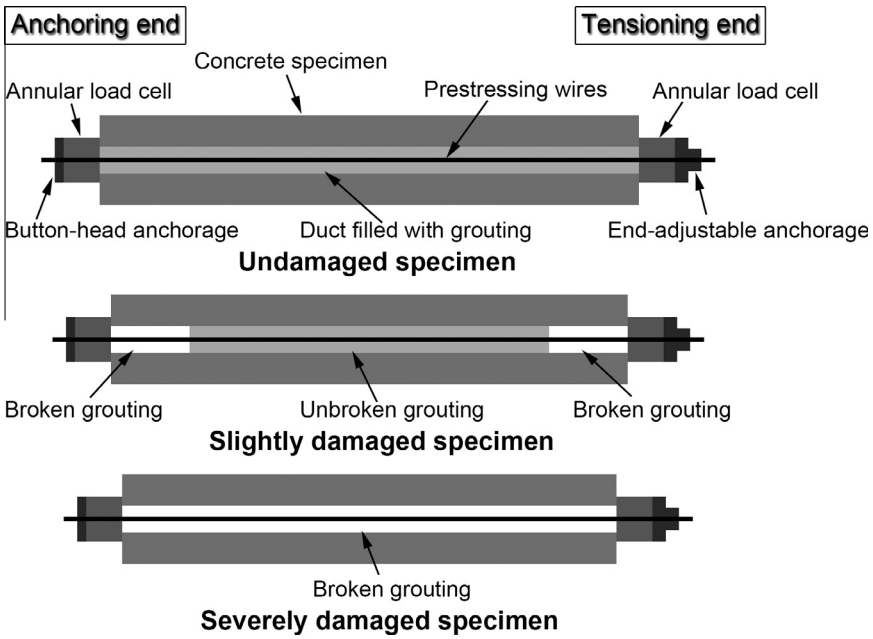

Fig. 15. Duct grouting of bonded prestressed specimen under the attack of FTCs.

Obviously, the friction forces do exist in the prestressed concrete specimens. The incompatible deformation between the prestressing wires and the concrete occurred after freeze-thaw attack. As shown in Fig. 13, the measured prestress losses of bonded specimen ($\Delta\sigma_{lF}^{A\text{-}b,\ \tau}$ and $\Delta\sigma_{lF}^{A\text{-}b,\ \alpha}$) are larger than that of unbounded specimen ($\Delta\sigma_{lF}^{A\text{-}u}$) as well as than the predictions. This could be caused by the effect of duct grouting. In the early stage of freeze-thaw attack, the cement paste at both ends of the duct started to be broken, which led to uneven deformation of the prestressing wires, as show in Fig. 15. Since in the middle part of duct the friction between the prestressing wires and the cement paste remain well, the deformation of the prestressing wires at this location will be smaller than that at both ends of duct under the attack of FTCs. Hence, the prestressed loss at middle of the concrete specimen is smaller than that at both ends. Besides, the friction forces between the grouting cement paste and the duct contribute to the difference between the measured prestress loss at the anchoring end and that at the tensioning end. As the FTCs are repeated, all the grouting cement paste in the duct will be broken completely and the uneven deformation of prestressing wires at the early stage of FTCs will eventually disappear. The measured prestress losses at the anchoring and tensioning ends after the 250th FTC were to some extent equal, as shown in Fig. 13.

The prestress losses measured after the 350th FTC, i.e. after the concrete material was completely ruptured, were about 5% of σ_{con}. And as shown in Fig. 13, a large deviation between predicted and measured results is shown after the 350th FTC. An inverse calculation according to the equations proposed in the previous work [2] suggests that the compressive strength of concrete dropped to about 10% and the Young's modulus has dropped to about 35% of their original values after the 350th FTC. The prestress force and the stirrups kept the crushed concrete together although the concrete had been completely damaged by FTCs.

5. Conclusions

This paper presents an effective method to investigate and evaluate the cracking and deformation of the pore structure inside the concrete under the attack of FTCs using RapidAir test system and metalloscope. Large spacing factor and small air content does not always result in poor durability of concrete. Obvious microscopic freeze-thaw damages, such as deeper crack, ITZ crack and ruptured pore edge, occurred after the 200th FTC, which indicates that severe freeze-thaw damage will occur and be aggravated after sufficient number of FTCs.

Although the concrete cubes, prisms and the prestressed specimens were made of the same concrete material and cast, cured and freeze-thawed under the same condition, quite different failure patterns were observed after the 350th FTCs. The main cause of this is that the external prestressing forces changed the stress state inside concrete material. The stress introduced by the external forces partly counterbalance or be superimposed on the freeze-induced tensile stress, which will change the cracks occurring and propagation in the prestressed concrete specimens. Therefore, different stress states of these concrete cubes, prims and the prestressed specimens result in different macroscopic rupture and failure patterns.

The RDME is only suitable for concrete slightly damaged by FTCs and cannot properly quantify the degradation of the mechanical properties of concrete seriously damaged by FTCs. However, the compressive strength of concrete is an appropriate macroscopic indicator to quantify freeze-thaw damage.

Normally the measurements of prestress losses of bonded specimen are larger than that of unbounded specimen because of the duct grouting effect. In bonded prestressed concrete specimens, the incompatible deformation between the prestressing wires and the concrete will occur after freeze-thaw damage. Moreover, the prestress loss at middle part of duct in the bonded prestressed concrete specimen is smaller than that at both ends at the early-stage of FTCs. However, all the grouting cement paste in the duct will eventually be ruptured with the FTCs being repeated, so the ultimate freeze-thaw prestress loss of the bonded specimen is approximately the same as that of the unbonded specimen.

The ultimate prestress loss due to FTCs reported in this test is approximately 50 MPa, around 5% of σ_{con}. A large deviation between prediction and measurements is observed after the 350th FTC because the mechanical properties of concrete after

the 350th FTC is not available. Inverse calculations indicate that the remaining compressive strength and Young's modulus in the core part might be slightly higher than 10% and 35% of their original values.

The freeze-thaw prestress loss should be classified as a time-dependent prestress loss. When evaluating the deflections or cracks of the concrete structures in cold regions, this prestress loss must be taken into account. It is suggested that the compressive strength of the freeze-thaw damaged concrete material should be measured, so that a more accurate freeze-thaw prestress loss would be available. In case the compressive strength is not measured, the ultimate freeze-thaw prestress loss should not be less than 5% of σ_{con} for safety concerns.

Acknowledgments

Funding for this experimental research work was provided by the National Natural Science Foundation of China (Project No. 50978224 and Project No. 51378104) and the Priority Academic Programme Development of Jiangsu Higher Education Institutions.

References

[1] M. Hasan, H. Okuyama, Y. Sato, T. Ueda, Stress-strain model of concrete damaged by freezing and thawing cycles, J. Adv. Concr. Technol. 2 (2004) 89–99.
[2] D.-F. Cao, X.-C. Qin, S.-P. Meng, Y.-M. Tu, L. Elfgren, N. Sabourova, et al., Evaluation of prestress losses in prestressed concrete specimens subjected to freezethaw cycles, Struct. Infrastruct. Eng. 12 (2016) 159–170.
[3] T.C. Powers, Working hypothesis for further studies of frost resistance of concrete, Am. Concr. Inst. J. 16 (1945) 245–272.
[4] F. Gong, E. Sicat, T. Ueda, D. Zhang, Meso-scale mechanical model for mortar deformation under freeze thaw cycles, J. Adv. Concr. Technol. 11 (2013) 49–60.
[5] S. Jacobsen, E.J. Sellevold, S. Matala, Frost durability of high strength concrete: effect of internal cracking on ice formation, Cem. Concr. Res. 26 (1996) 919–931.
[6] S. Jacobsen, J. Marchand, H. Hornain, SEM observations of the microstructure of frost deteriorated and self-healed concretes, Cem. Concr. Res. 25 (1995) 1781–1790.
[7] Z. Yang, W.J. Weiss, J. Olek, Water transport in concrete damaged by tensile loading and freeze-thaw cycling, J. Mater. Civ. Eng. 18 (2006) 424–434.
[8] L. Liu, D. Shen, H. Chen, W. Sun, Z. Qian, H. Zhao, et al., Analysis of damage development in cement paste due to ice nucleation at different temperatures, Cem. Concr. Compos. 53 (2014) 1–9.
[9] M. Pigeon, C. Talbot, J. Marchand, H. Hornain, Surface microstructure and scaling resistance of concrete, Cem. Concr. Res. 26 (1996) 1555–1566.
[10] S. Jacobsen, H. Christian Gran, E.J. Sellevold, J.A. Bakke, High strength concrete-freeze/thaw testing and cracking, Cem. Concr. Res. 25 (1995) 1775–1780.
[11] W. Li, W. Sun, J. Jiang, Damage of concrete experiencing flexural fatigue load and closed freeze/thaw cycles simultaneously, Constr. Build. Mater. 25 (2011) 2604–2610.
[12] S. Li, G. Chen, G. Ji, Y. Liu, Quantitative damage evaluation of air-entrained concrete suffered freezing-thawing by digital-image-processing technique, Kuei Suan Jen Hsueh Pao/J. Chin. Ceram. Soc. 42 (2014) 951–959.
[13] S. Diamond, Mercury porosimetry. An inappropriate method for the measurement of pore size distributions in cement-based materials, Cem. Concr. Res. 30 (2000) 1517–1525.
[14] E. Sicat, F. Gong, D. Zhang, T. Ueda, Change of the coefficient of thermal expansion of mortar due to damage by freeze thaw cycles, J. Adv. Concr. Technol. 11 (2013) 333–346.
[15] F. Gong, E. Sicat, D. Zhang, T. Ueda, Stress analysis for concrete materials under multiple freeze-thaw cycles, J. Adv. Concr. Technol. 13 (2015) 124–134.
[16] T. Suzuki, H. Ogata, R. Takada, M. Aoki, M. Ohtsu, Use of Acoustic Emission and X-ray Computed Tomography for Damage Evaluation of Freeze-thawed Concrete, 12th ed., Elsevier Ltd, Langford Lane, Kidlington, Oxford, OX5 1GB, United Kingdom, 2010, pp. 2347–2352.
[17] H. Shang, Y. Song, Experimental study of strength and deformation of plain concrete under biaxial compression after freezing and thawing cycles, Cem. Concr. Res. 36 (2006) 1857–1864.
[18] H. Shang, Y. Song, L. Qin, Experimental study on the property of concrete after freeze-thaw cycles, China Concr. Cem. Prod. 32 (2005) 9–11.
[19] H. Shang, Y. Song, L. Qin, Experimental study on strength and deformation of plain concrete under triaxial compression after freeze-thaw cycles, Build. Environ. 43 (2008) 1197–1204.
[20] H. Shang, Q. Yin, Y. Song, L. Qin, Experimental study on the influence of freezing and thawing cycles on deformation features of common concrete, Yangtze River 39 (2006) 60–63.
[21] A. Duan, W. Jin, J. Qian, Effect of freeze–thaw cycles on the stress–strain curves of unconfined and confined concrete, Mater. Struct. 44 (2011) 1309–1324.
[22] M. Hasan, T. Ueda, Y. Sato, Stress-strain relationship of frost-damaged concrete subjected to fatigue loading, in: Special Issue: Durability and Service Life of Concrete Structures: Recent Advances, first ed., American Society of Civil Engineers, 1801 Alexander Graham Bell Drive, Reston, VA 20191-4400, United States, 2008, pp. 37–45.
[23] B. Diao, Y. Sun, S. Cheng, Y. Ye, Effects of mixed corrosion, freeze-thaw cycles, and persistent loads on behavior of reinforced concrete beams, J. Cold Reg. Eng. 25 (2011) 37–52.
[24] K. Zandi Hanjari, P. Kettil, K. Lundgren, Modelling the structural behaviour of frost-damaged reinforced concrete structures, Struct. Infrastruct. Eng. 9 (2013) 416–431.
[25] M. Hassanzadeh, G. Fagerlund, Residual strength of the frost-damaged reinforced concrete beams, in: III European Conference on Computational Mechanics, Springer, 2006, p. 366.
[26] D. Cao, X. Qin, S. Yuan, Experimental study on mechanical behaviors of prestressed concrete beams subjected to freeze-thaw cycles, Tumu Gongcheng Xuebao/China Civ. Eng. J. 46 (2013) 38–44.
[27] RapidAir-457, User's Manual – Version 3.0: Concrete Experts International ApS, 2013.
[28] ASTM, Standard Test Method for Resistance of Concrete to Rapid Freezing and Thawing, 2008.
[29] D. Cao, L. Fu, Z. Yang, X. Qin, Relationship between mechanical properties and relative dynamic elasticity modulus of concrete after freeze-thaw cycles, Jiangsu Daxue Xuebao (Ziran Kexue Ban)/J. Jiangsu Univ. (Nat. Sci. Ed.) 33 (2012) 721–725.
[30] D.-F. Cao, L.-Z. Fu, Z.-W. Yang, X.-C. Qin, Study on constitutive relations of compressed concrete subjected to action of freezing-thawing cycles, Jianzhu Cailiao Xuebao/J. Build. Mater. 16 (2013). 17–23+32.
[31] MOHURD, Standard for test methods of long-term performance and durability of ordinary concrete, 2009.
[32] S. Jacobsen, E.J. Sellevold, Self healing of high strength concrete after deterioration by freeze/thaw, Cem. Concr. Res. 26 (1996) 55–62.
[33] D. Cao, L. Fu, Z. Yang, X. Qin, Study on constitutive relations of compressed concrete subjected to action of freezing-thawing cycles, Jianzhu Cailiao Xuebao/J. Build. Mater. 16 (2013). 17–23+32.